The 2022 World Congress on
Advances in Civil, Environmental, & Materials Research (ACEM22)
16-19, August, 2022, GECE, Seoul, Korea

Ultimate and fatigue strength analysis of a steel-UHPFRC hybrid tower for offshore wind turbines

*Chao Chen[1)], Xiujiang Shen[2)], Xugang Hua[3)] and Xudong Shao[4)]

[1), 2 , 3 , 4)] *Key Laboratory for Wind and Bridge Engineering, Hunan University, Changsha, China*
[1), 2 , 3 , 4)] *College of Civil Engineering, Hunan University, Changsha, China*

[1)] steinchen@hnu.edu.cn

ABSTRACT

This study proposes a steel-Ultra-High-Performance Fibre-Reinforced Concrete (UHPFRC) hybrid tubular tower to support Offshore Wind Turbines (OWTs). This hybrid tower composes a reinforced UHPFRC tube at the bottom, a steel tube at the top and a standard steel tube monopile below the mudline. With carefully selected geometric parameters, the hybrid tower is designed to support a DTU 10 MW rotor. A simplified method is proposed to estimate the ultimate strength of the reinforced UHPFRC tube section, while a method based on the SN curve and crack width limit is used to check its fatigue strength. It is found that the hybrid tower has enough ultimate strength a much longer fatigue life compared to a reference steel tube tower. In the meantime, the total material cost of the hybrid tower is found to be only 58% of that of the reference steel tube tower.

1. INTRODUCTION

Reducing the cost for wind turbine support structures is very important to make offshore energy more economic. At present, most wind turbine towers are made of steel, which are vulnerable to fatigue damages and corrosion in the harsh ocean environment. Therefore, it is valuable to design wind turbine towers with new materials so that these towers have a better resistance to environmental loads and longer useful life. Characterised by its high strength and durability, UHPFRC is a notable representative of construction materials which are able to resist the threat of corrosion by seawater (Chen *et al.*, 2018). However, only limited studies can be found in the

---

[1)] Postdoctoral Researcher
[2)] Postdoctoral Researcher
[3)] Professor
[4)] Professor

literature where attempts were made to use UHPFRC to construct support structures for OWTs (Jammes, 2009; Wu, Yang and Mpalla, 2013; Ma and Yang, 2020). On the other hand, the hybrid-tower concept for wind turbines, which usually combines an upper steel part and a lower concrete part, has been attracting interests from researchers. This is because hybrid wind turbine towers have larger flexural stiffness and the upper can steel take the advantage of easier prefabrication and assembling, compared to traditional steel tower (J. Chen *et al.*, 2021). Combining the hybrid-tower concept and UHPFRC as a new material, this study investigates the feasibility of hybrid steel-UHPFRC tower for large-size offshore wind turbines, by evaluating the ultimate and fatigue strength of a reinforced UHPFRC tube as the lower part of the hybrid tower.

2. Overview of the hybrid support structure

A hybrid tower is designed to support a DTU 10 MW wind turbine (Bak *et al.*, 2013). The tower top height is 119 m from the Mean Sea Level (MSL), and the water depth is 30 m. This hybrid tower combines a reinforced UHPFRC tube at the bottom and a steel tube at the top, and a steel monopile below the mudline, as shown in Fig. 1(a). For comparison, a steel tube including a variable-section part above the MSL and a constant-section part below the MSL is used as a reference tower, as shown in Fig. 1(b). This reference tower is taken from the study by (Yang *et al.*, 2020). Both the hybrid and reference towers are mounted on a 40-metre steel monopile under the mudline. The soil around the steel monopile is assumed to be medium-dense sand. The basic properties of the DTU 10 MW wind turbine and steel monopile are listed in Table 1. A coordinate system is defined in Fig. 1, with x and y axes pointing to the fore-aft and side-side directions respectively. z axis is vertically upward.

Table 1 Properties of the DTU 10 MW reference offshore wind turbine

Rated power (MW)	10
Cut-in/cut-out speeds (m/s)	4/25
Rated wind speed (m/s)	11.4
Rotor diameter (m)	178.3
Hub height (m)	119
Nacelle and hub mass (kg)	551,556
Rotor mass (kg)	41,716
Steel monopile length (m)	40
Steel monopile diameter (m)	9
Steel monopile thickness (mm)	110

To design the hybrid tower, it first requires determining its geometric properties, including the diameters and thicknesses of both the reinforced-UHPFRC tube and the steel tube. As this paper focuses on the performance of the reinforced UHPFRC tube, the section dimensions of the steel tube in the hybrid tower are the same as those of the steel tube in the reference tower for the same height. The length of the UHPFRC tube is selected as half of the length of the hybrid tower above the mudline. Additionally, for simplicity the diameter of the top section of the UHPFRC tube is the same as the

bottom section of the steel tube. The geometric properties of the hybrid tower and reference tower are presented in Table 2 and Table 3 respectively.

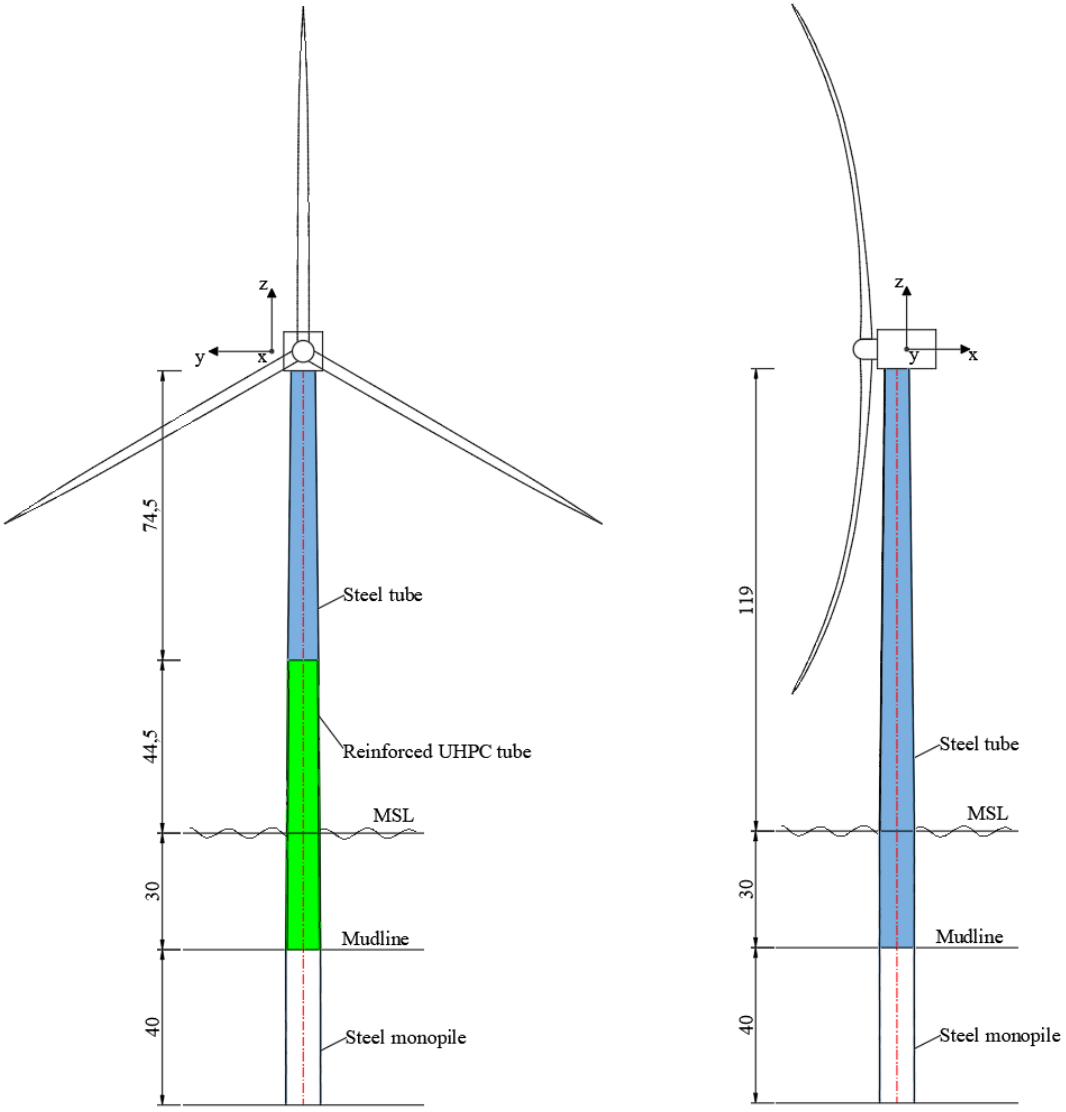

(a) (b)

Fig. 1 Schematics of the DTU 10 MW OWTs supported by the hybrid tower (a) and the reference tower (b).

Table 2 Geometric properties of the hybrid tower

Steel tube		**UHPFRC tube**	
Length (m)	74.5	Length (m)	74.5
Top diameter (m)	6.25	Top diameter (m)	7.97
Bottom diameter (m)	7.97	Bottom diameter (m)	9
Top thickness (mm)	35	Top thickness (mm)	300

Bottom thickness (mm)	54.7	Bottom thickness (mm)	400

Table 3 Geometric properties of the reference tower

Steel tube above MSL		**Steel tube below MSL**	
Length (m)	119	Length (m)	30
Top diameter (m)	6.25	Diameter (m)	9
Bottom diameter (m)	9	Top thickness (mm)	110
Top thickness (mm)	35		
Bottom thickness (mm)	66.5		

The UHPFRC contains 3.8% by volume of straight steel fibers with length of 13 mm and diameter of 0.175 mm, and its water to cement ratio is 0.15. The rebars in the reinforced UHPFRC tube are made of steel with grade of D500. The reinforcement ratio of the UHPFRC tube for the vertical rebars should be carefully designed and optimised in real design practice to ensure the reinforced section is cost-effective and simultaneously has enough resistance. However, the reinforcement ratio in this paper is kept as 1% for simplicity since this paper focuses on the feasibility of the hybrid tower. The steel tubes in the hybrid tower and reference tower are both made of steel S355. The material properties of the reinforced UHPFRC tube and the steel tube are listed in Table 4.

Table 4 Material properties of reinforced UHPFRC, steel and

Reinforced UHPFRC tube				**Steel tube**	
UHPFRC		**Rebar**			
Density (kg/m^3)	2700	Density (kg/m^3)	7850	Density (kg/m^3)	7850
Young's modulus (GPa)	48	Young's modulus (GPa)	200	Young's modulus (GPa)	210
Poisson's ratios	0.2	Poisson's ratios	0.3	Poisson's ratios	0.3
Shear modulus (GPa)	20	Shear modulus (GPa)	76.9	Shear modulus (GPa)	80.3
Compressive strength (MPa)	150	Yield strength (MPa)	500	Yield strength (MPa)	355
Ultimate tensile strength (Mpa)	12				

To evaluate the economic benefits, the costs for materials in the hybrid tower and reference tower are estimated and compared. The price of steel is set as 10000 ¥/ton including the costs for raw material and labour, and the price of UHPFRC is set as 2500 ¥/ton, according to the data provided in (Ma and Yang, 2020). Given the weights of steel and UHPFRC, the total price of the hybrid tower is 1.1×10^7 ¥, while the total price of the reference tower is 1.9×10^7 ¥. Therefore, the total material cost of the hybrid tower is only 58% of that of the reference steel tube tower.

3. Aeroelastic FE model and load cases

2.1 Aeroelastic model description

To calculate the modal properties and dynamic responses of the hybrid tower, a fully coupled aeroelastic model was coded in Matlab. This model is an updated version of the numerical model presented in the authors' previous study (C. Chen *et al.*, 2021). This aeroelastic model is a FE formulation including the blades, tower and monopile represented by soil springs lumped at the mudline. This aeroelastic model can easily include soil-structure interaction and model the hybrid tower, simultaneously taking advantage of the improved accuracy of the FE formulation.

In the FE model, the tower and blades were modelled using three-dimensional Euler-Bernoulli beam elements. The numbers of beam elements for the single blade and tower are 37 and 25 respectively, so the total number of beam elements is 136. A convergence study confirmed that the beam element number is sufficient. Given the material and geometrical properties of the beam elements, the equations of motion of the FE model are:

$$\mathbf{M}\ddot{\mathbf{u}} + (\mathbf{C}_{Struc} + \mathbf{C}_{Soil})\dot{\mathbf{u}} + \mathbf{K}\mathbf{u} = \mathbf{F}_{Wind} + \mathbf{F}_{Wave}, \quad (1)$$

where $\mathbf{M}, \mathbf{K}$ are the mass and stiffness matrices, $\mathbf{C}_{Struc}$ and $\mathbf{C}_{Soil}$ are the structural damping and soil damping matrices respectively, $\mathbf{u}$ is the displacement vector, $\mathbf{F}_{Wind}$ and $\mathbf{F}_{Wave}$ are the wind force and wave force vectors. The structural damping and soil damping in this study are both assumed to be proportional Rayleigh damping. The total damping ratios due to the structural damping and soil damping are 2.0% according to (Chen and Duffour, 2018). The structural damping of a single blade was set to 0.48% according to (Bak *et al.*, 2013). The hydrodynamic damping and aerodynamic damping of the tower were not included as their contributions are small compared to other damping sources. The nacelle and hub were modelled using a lumped mass at the tower top, added to the mass matrix. Time domain analyses were conducted by implementing the numerical integration scheme HHT-α, which is a generalised version of the Newmark-β method.

The wind loading on the rotor is calculated by unsteady Blade Element Momentum (BEM) theory with corrections (Hansen, 2008). The corrections adopted in the unsteady BEM code include Prandtl and Glauert corrections. Other corrections such as skew wake and dynamic wake corrections are not included in the unsteady BEM code for simplicity. The wind loading on the tower is also considered. The Kaimal spectrum was used to generate turbulent wind fields, and its relevant parameters (e.g., coherence length parameters) were selected as recommended by IEC 61400-3 (International Electrotechnical Commission (IEC), 2009). Medium turbulence intensity (Category B) was assumed. The inflow wind velocities, the velocity caused by rotor rotation and the velocities caused by blade vibration were used as input to the unsteady BEM code. The unsteady code calculates the instantaneous local aerodynamic forces for all blade elements at every time step in the time integration.

Wave loading calculation is based on Morison's equation. The drag coefficient and inertia coefficient were chosen as 1 and 2 respectively as the recommended values in (Shirzadeh *et al.*, 2013). The velocities caused by monopile vibration were ignored in the wave loading calculation as the monopile vibration velocities are much smaller than the wave particle velocities. The wave profile is irregular and obtained by the

superposition of wave components following linear wave theory and JONSWAP spectrum (Hasselmann *et al.*, 1973).

The steel monopile is assumed to be surrounded by a single layer of sand in this study. The saturated soil weight is 20 kN/m^3 and the internal friction angle is 36º. The SSI was modelled by a simplified method in which lumped springs at the mudline to accelerate the fatigue analysis. This method assumes a stiff monopile. The stiffness coefficients are calculated based on the method described in (Darvishi-Alamouti, Bahaari and Moradi, 2017; Wang, Larsen and Bredmose, 2021). The lateral stiffness K_{uu}, the rotational stiffness $K_{\theta\theta}$ and the cross-coupling stiffness $K_{u\theta}$ are determined by

$$\begin{bmatrix} K_{uu} & K_{u\theta} \\ K_{u\theta} & K_{\theta\theta} \end{bmatrix} = \begin{bmatrix} \frac{1}{2}L_p^2 n_h & -\frac{1}{3}L_p^3 n_h \\ -\frac{1}{3}L_p^3 n_h & \frac{1}{4}L_p^4 n_h \end{bmatrix}, \quad (2)$$

where L_p is the length of the steel monopile, n_h is a coefficient of subgrade reaction constant with depth. n_h is taken as 5000 kN/m^3 for medium dense sand according to (Wang, Larsen and Bredmose, 2021). It is assumed that the top of the steel monopile is unable to move vertically and rotate around z axis.

2.1 Load cases

To study the capacities of the hybrid tower against large environmental loads, it needs to define critical environmental states and corresponding load cases to cover both operating and parked conditions. Here the selection of load cases is according to the IEC 61400-3 offshore wind turbine design standard (International Electrotechnical Commission (IEC), 2009). To conduct the ultimate strength analysis, DLC1.1 and DLC6.1 are selected. DLC1.1 considers operating OWT under normal turbulent winds and normal waves. The metocean data used in this paper is based on the data provided in (Velarde *et al.*, 2020). For DLC1.1, wind speeds from 5 m/s to 25 m/s in 2 m/s steps with the normal turbulent intensity I_n are listed in Table 5. For every wind speed, the peak wave periods and significant wave height are picked for normal sea state and severe sea state respectively. Additionally, DLC6.1 considers idling or parked wind turbines subjected to extreme wind and wave loads with a 50-year return period. DLC6.1 is analysed under a reference wind speed of 45.8 m/s as provided in (Wang, Larsen and Bredmose, 2021), with wind turbulence and wave parameters listed in the bottom of Table 5.

Table 5 Environmental states

Wind condition		**Wave condition**		
V_w (m/s)	I_n (%)	T_p (s)	H_s (m)	P_j (%)
5	26.2	6.8	0.82	5.3
7	21.7	7.0	1.01	10.4
9	19.2	7.1	1.24	15.2
11	17.6	7.4	1.55	17.9
13	16.5	7.8	2.01	17.1
15	15.7	8.2	2.53	13.0
17	15.1	8.9	3.07	9.2

19	14.6	9.9	3.65	5.5
21	14.2	10.4	4.08	3.0
23	13.9	11.4	4.76	1.6
25	13.6	12.9	5.40	0.7
45.8	11.0	13.8	9.9	-

For the fatigue analysis, DLC1.2 corresponding to normal operation condition is selected. Grouped into 2 m/s bins, wind speeds from 5 m/s to 25 m/s with normal turbulence are also selected for the fatigue analysis, together with a normal sea state. To determine the long-term joint distribution of the wind and wave conditions, a two-parameter Weibull distribution was used according to the study by Velarde et al. (Velarde *et al.*, 2020). 13 environmental states were used to conduct the fatigue analysis. 92% of probability of occurrence is for the operational environmental states.

The wind and wave directionality in this study was simplified by assuming the wind and wave loads are in the same direction, and yaw error is not considered as this study aims at providing a preliminary performance assessment of the hybrid tower under representative environmental states. To represent the influence of the OWT control, a standard relationship between the mean wind speed, rotor rotation speed and blade pitch angles was used according to (Bak *et al.*, 2013).When the OWT is parked, it is assumed the pitch angle is 90 ^{o} with zero rotational speed.

4. Results

2.1 Natural frequency

The natural frequencies of OWT towers should be kept far away from the resonance ranges caused by periodic wave loads and well known 1P Sand 3P rotor frequencies. With the developed aeroelastic models, the natural frequencies of the wind turbine can be calculated. For the hybrid tower, the natural frequencies of the first two bending modes in the FA direction are 0.25 Hz and 1.2 Hz respectively. While for the reference tower, these two natural frequencies are 0.26 Hz and 1.37 Hz. The first natural frequencies are very close for these two towers, but a slight frequency difference can be found for the second mode. The natural frequencies of the hybrid tower and reference tower are both in the soft-stiff range and away from the rotor frequency and wave frequency ranges, indicating that the designs of the two towers are safe.

2.2 Ultimate strength

The ultimate strength analysis for the hybrid tower requires determination of the ultimate resistance of the reinforced UHPFRC section. The reinforced UHPFRC section is similar to a conventional reinforced concrete section, so a method developed from the ACI code for reinforced concrete chimneys (American Concrete Institute, 2008) is proposed to estimate the ultimate resistance of the reinforced UHPFRC section under axial force and bending. This method assumes a linear strain distribution when the section reaches its maximum resistance. The stresses of the UHPFRC and steel rebars are calculated by dividing the section into strips, given the stress-strain relationships of

steel and UHPFRC. With an initial guess of the strain at the section edge and the position of the neutral axis, it can find the maximum moment resistance given an axial loading. The strain-stress relationships for UHPFRC and steel rebar are shown in Fig. 2, with critical values listed in Table 6.

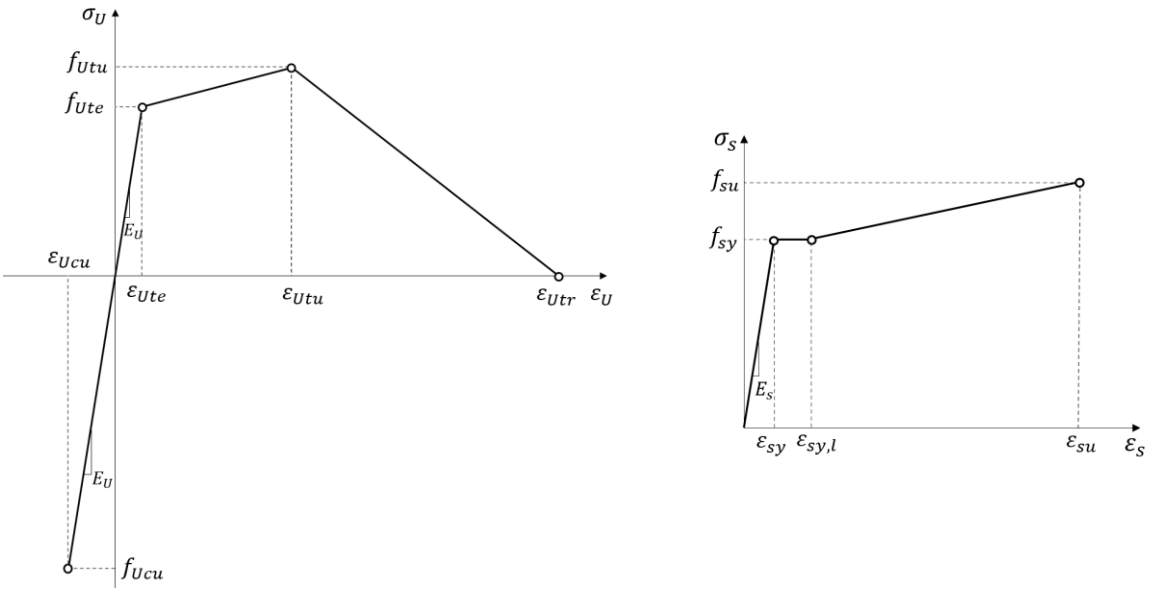

(a) (b)

Fig. 2. Strain-stress relationship for UHPFRC (a) and steel rebar (b).

Table 6 Critical strain and stress values for UHPFRC and steel rebar

UHPFRC		**Steel rebar**	
f_{Ute} (MPa)	8	f_{sy} (MPa)	500
ε_{Ute} (%)	0.0167	ε_{sy} (%)	0.25
f_{Utu} (MPa)	12	$\varepsilon_{sy,l}$ (%)	2.5
ε_{Utu} (%)	0.2	f_{su} (MPa)	565
ε_{Utr} (%)	1	ε_{su} (%)	15
f_{Ucu} (MPa)	150		
ε_{Ucu} (%)	0.3125		

As an OWT tower can be regarded as a cantilever supported by soil springs at the mudline (Adhikari and Bhattacharya, 2012), the largest moment can be usually found at the bottom section at the mudline. this paper assumes the maximum moment occurs at the section at the mudline for the purpose of a feasibility study. To calculate the ultimate strengths of the reinforced UHPFRC section and the steel tube section, it first requires determining the axial loading. According to simulation results for DLC1.1 and DLC6.1, the axial loading slightly fluctuates around the total gravitational load caused by the RNA mass and tower mass. Thus, the design axial loading can be regarded as the total gravitational load. For the hybrid tower, the total gravitational load for the section at the mudline is 35.9 MN, while for the reference tower this gravitational load is 25 MN. By using the estimation methods given in Section 6.2, the calculated

ultimate strength for the reinforced UHPFRC tube section at the mudline is 505 MN·m. For the reference tower, and the ultimate strength of the steel tube section at the mudline is 1545 MN·m by using the method recommended by DNV-GL (DNVGL, 2019). Therefore, the ultimate strength of the reinforced UHPFRC section is much less than that of the steel tube section.

The ultimate design loads were determined by the numerical simulations for DLC1.1 and DLC6.1 considering different combinations of winds and waves and random seeds. Given a mean wind speed and a random seed, the maximum bending moments at the tower bottom section can be obtained from the time series of internal forces. For each mean wind speed, the mean value and standard deviation were calculated from the maximum bending moments corresponding to the 6 random seeds. Fig. 3 compares the calculated mean values and standard deviations of the maximum bending moments in the hybrid tower and reference tower for different mean wind speeds. The maximum bending moments for the hybrid tower and reference tower are generally close for different mean wind speeds. When the OWTs are operating at the rated wind speed, the mean value and standard deviation of the maximum bending moments are 429 MN·m and 11 MN·m for the hybrid tower, which are slightly smaller than those values (433 MN·m and 13 MN·m, respectively) for the reference tower. The maximum bending moments become smaller for other mean wind speeds. When the OWTs are parked and subjected to extreme wind, the mean value and standard deviation of the maximum bending moment for the hybrid tower are 433 MN·m and 42 MN·m, which are smaller than those for the reference tower. According to all the simulation results, the maximum design moment for the hybrid tower is 473 MN·m which is less than the ultimate strength of 505 MN·m, meaning that the design of the reinforced UHPFRC section is safe. In addition, the hybrid tower has a slightly smaller design bending moment compared to the reference tower.

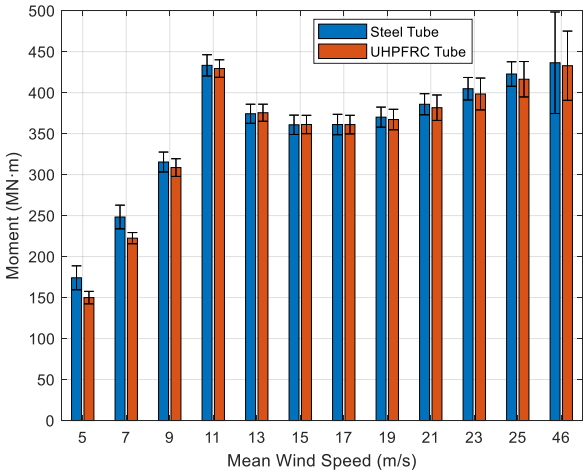

Fig. 3 Mean values and standard deviations of the maximum bending moments at the mudline for the hybrid tower and reference tower.

2.3 Fatigue strength

Currently, there is no widely accepted S-N curve for UHPFRC in tension due to the limited studies and experimental data. Similar as steel, UHPFRC shows a fatigue endurance limit, above which fatigue stress induces significant damage leading to fracture failure. Based on the data provided by (Makita and Brühwiler, 2014b), (Loraux, 2018) and (Shen and Brühwiler, 2020), the tensile and compressive fatigue S-N curves for unreinforced UHPFRC are plotted in red and green in Fig. 4(a). The standard S-N curve for steel according to ((DNV) Det Norske Veritas, 2005) is also plotted in Fig. 4(a). Furthermore, it was indicated experimentally that the tensile fatigue endurance limit in tension could be improved to a stress level that UHPFRC is in the strain-hardening domain with steel reinforcement (Makita and Brühwiler, 2014a). As the number of fatigue cycles increases, it was found the stress gradually transfers from UHPFRC to steel rebars. Therefore, the final fatigue strength of reinforced UHPFRC is dependent on the rebars' ability to resist fatigue damages. As there is no experimental study for the fatigue behaviour of reinforced UHPFRC tube section under axial force and bending moment, the S-N curve obtained by (Makita and Brühwiler, 2014a) for rebars in a reinforced UHPFRC layer to strengthen a bridge deck slab was selected to evaluate the fatigue strength of the reinforced UHPFRC tube section. This S-N curve is plotted in blue in Fig. 4(b), compared to the S-N curve for a single rebar.

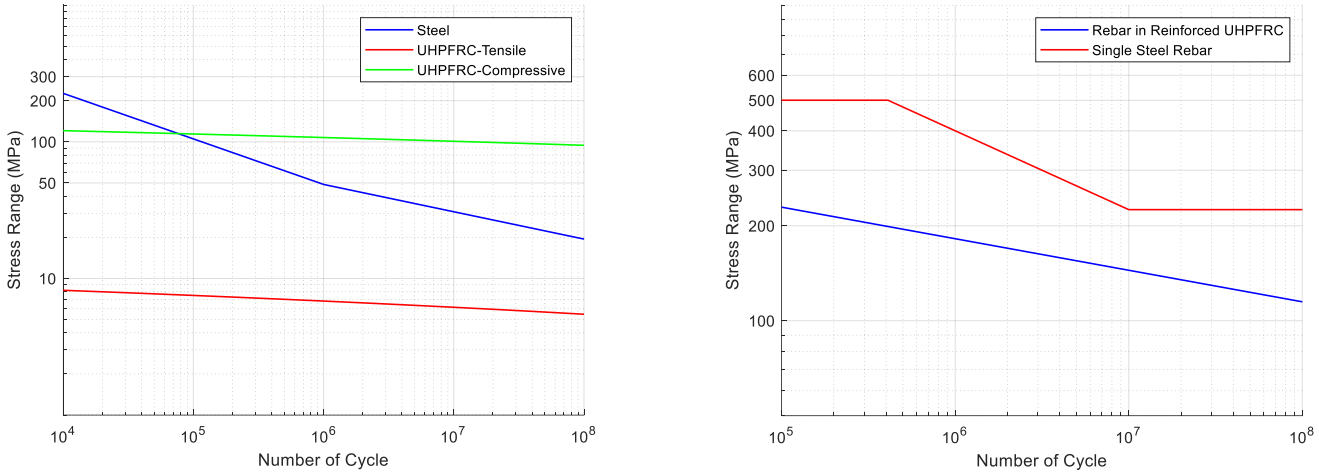

Fig. 4. Compressive and tensile fatigue S-N curves for unreinforced UHPFRC, S-N curve for steel tube (a); tensile fatigue S-N curves for rebars in reinforced UHPFRC and a single steel rebar (b).

Similar to the ultimate strength analysis, the fatigue strengths of the hybrid tower and the reference tower were only checked for the reinforced UHPFRC tube section and the steel tube section at the mudline. The time domain simulations conducted for DLC1.1 can also be used to conduct fatigue analysis for DLC1.2 as the combinations of winds and waves are the same for these two load cases. Given the axial force and the bending moments about the x and y axes respectively, the longitudinal stress in the at an arbitrary position at the tube section can be calculated. For the reinforced

UHPFRC section, all the rebars were regarded located at the middle of the circular section for simplicity and the stress distribution for the UHPFRC and rebars was considered by assuming a linear strain distribution along the section.

For each mean wind speed, the mean value and standard deviation of the maximum stress ranges for UHPFRC and rebars can be obtained from the stress time series given 6 random seeds. These maximum stress ranges are illustrated in Fig. 5(a), showing that the maximum stress range increases with the mean wind speed. The averaged maximum stress range for UHPFRC grows from 4.9 MPa to 15.6 MPa when the mean wind speed changes from 5 m/s to 25 m/s. According to the compressive S-N curve for unreinforced UHPFRC, the minimum stress range under which the fatigue failure of UHPFRC requires more than 10^8 circles is 94.4 MPa. Thus, the compressive fatigue endurance of the reinforced UHPFRC tube section can be found to be infinite as the maximum compressive stress range is only 15.6 MPa.

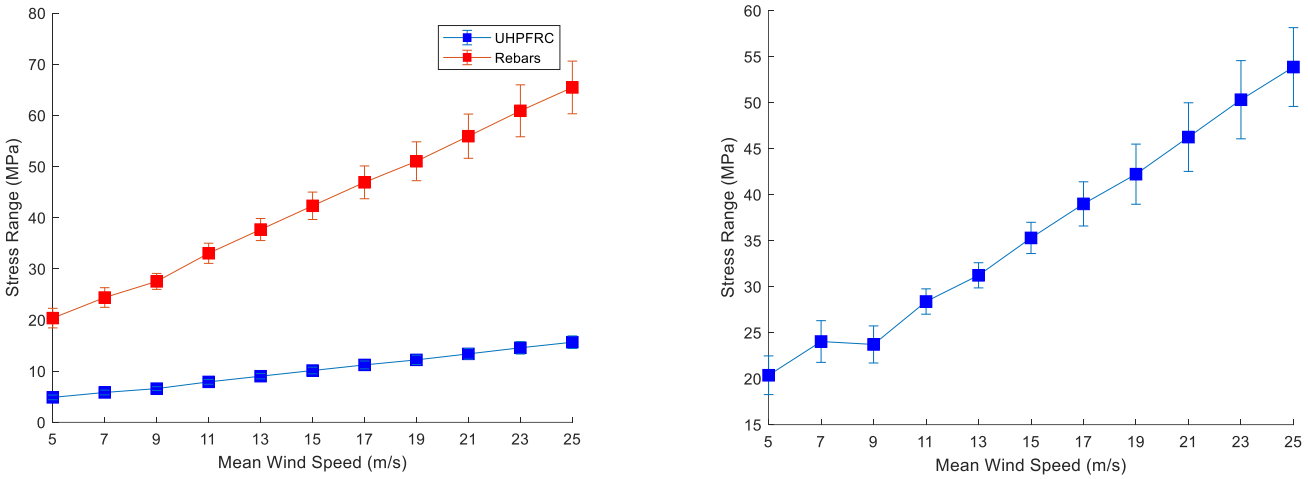

Fig. 5. Maximum stress ranges for UHPFRC and rebars in the UHPFRC section (a); maximum stress ranges for steel in the reference steel section (b).

The effect of reinforcement on the fatigue strength of the reinforced UHPFRC tube section must be considered. Fig. 5(a) also shows the averaged maximum stresses range for the rebars increasing from 20.4 MPa to 65.5 MPa with the increase of the mean wind speed. According to the tensile fatigue S-N curve for rebars given in Fig. 4(b), it requires more than 10^8 circles to cause a tensile fatigue failure of the rebars if the stress range is less than 115.1 MPa. Therefore, the rebars' maximum stress range of 65.5 MPa leads to a very good fatigue endurance.

For the refence steel tube section at the mudline, the mean value and standard deviation of the maximum stress ranges for the reference steel tube section were calculated and given in Fig. 5(b). With the simulation results for DLC1.2, the fatigue life predictions can be done for the reinforced UHPFRC tube section in the hybrid tower

based on different curves, and for the steel tube section in the reference tower. Combining the fatigue damage summing rule and the occurrence probability for each mean wind speed, the fatigue life predictions were conducted, and the results are shown in Table 7. It shows that the fatigue life of the hybrid tower is nearly infinite if assuming the fatigue resistance of the reinforced UHPFRC tube is dependent on the fatigue life of the rebars, while the fatigue life of the reference steel tube is only 55.8 years.

Table 7 Fatigue life estimations for the reinforced UHPFRC tube section and the steel tube section

	Fatigue life (year)
UHPFRC with the tensile S-N curve	4×10^{-12}
UHPFRC with the compressive S-N curve	6×10^{14}
Rebars	1.4×10^{7}
Reference steel tube	55.8

5. CONCLUSIONS

In this study, a steel-UHPFRC hybrid tower is proposed to support a 10 MW DTU reference OWT. The ultimate and fatigue strengths of the reinforced UHPFRC tube are studied under different operational and environmental conditions, and the results are compared to those for a reference steel tube. It was found that the UHPFRC tube has lower ultimate strength compared to the reference tower but can still satisfy the design requirements for ultimate strength. Moreover, the fatigue life of the UHPFRC tube is found to be much longer than that of the reference tower. The natural frequencies of the hybrid tower and reference tower are very close, but the material cost of the hybrid tower is much lower. In conclusion, the hybrid steel-UHPFRC tower has the potential to be a good alternative to the conventional steel tower due to its lower cost, higher fatigue and corrosion resistance, and sufficient ultimate strength.

REFERENCES

Adhikari, S. and Bhattacharya, S. (2012) “Dynamic analysis of wind turbine towers on flexible foundations,” *Shock and Vibration Digest*, **19**(1), pp. 37–56.

American Concrete Institute (2008) *Code requirements for reinforced concrete chimneys (ACI 307-08) and Commentary*. ACI 307-08.

Bak, C. *et al.* (2013) “Description of the DTU 10 MW reference wind turbine.”

Chen, C. *et al.* (2021) “Numerically efficient fatigue life prediction of offshore wind turbines using aerodynamic decoupling,” *Renewable Energy*, **178**, pp. 1421–1434.

Chen, C. and Duffour, P. (2018) “Modelling damping sources in monopile-supported offshore wind turbines,” *Wind Energy*. Wiley, **21**(11), pp. 1121–1140.

Chen, J. *et al.* (2021) “Seismic response analysis of steel–concrete hybrid wind turbine tower,” *Journal of Vibration and Control*. SAGE Publications Ltd STM, p. 10775463211007592.

Chen, Y. *et al.* (2018) “Evaluation and optimization of Ultra-High Performance Concrete (UHPC) subjected to harsh ocean environment: Towards an application of Layered

Double Hydroxides (LDHs)," *Construction and Building Materials*. Elsevier, **177**, pp. 51–62.

Darvishi-Alamouti, S., Bahaari, M.-R. and Moradi, M. (2017) "Natural frequency of offshore wind turbines on rigid and flexible monopiles in cohesionless soils with linear stiffness distribution," *Applied Ocean Research*. Elsevier, **68**, pp. 91–102.

(DNV) Det Norske Veritas (2005) "Fatigue Design of Offshore Steel Structures," *Recommended Practice DNV-RPC203*, (October), p. 126.

DNVGL (2019) *DNVGL-RP-C202 - Buckling strength of shells*. DNVGL-RP-C202.

Hansen, M. O. L. (2008) *Aerodynamics of wind turbines*. 3rd ed. London, England: Routledge.

Hasselmann, K. *et al.* (1973) "Measurements of wind-wave growth and swell decay during the Joint North Sea Wave Project (JONSWAP)," *Ergnzungsheft zur Deutschen Hydrographischen Zeitschrift Reihe*, **A**(8), pp. 1–95.

International Electrotechnical Commission (IEC) (2009) "IEC 61400-3 Wind turbines - Part 3: Design requirements for offshore wind turbines."

Jammes, F.-X. (2009) *Design of wind turbines with Ultra-High Performance Concrete*. Massachusetts Institute of Technology.

Loraux, C. T. (2018) *Long-term monitoring of existing wind turbine towers and fatigue performance of UHPFRC under compressive stresses*. Ecole Polytechnique Fédérale de Lausanne.

Ma, H. and Yang, J. (2020) "A novel hybrid monopile foundation for offshore wind turbines," *Ocean Engineering*. Elsevier Ltd, **198**(May 2019), p. 106963.

Makita, T. and Brühwiler, E. (2014a) "Tensile fatigue behaviour of Ultra-High Performance Fibre Reinforced Concrete combined with steel rebars (R-UHPFRC)," *International journal of fatigue*. Elsevier, **59**, pp. 145–152.

Makita, T. and Brühwiler, E. (2014b) "Tensile fatigue behaviour of ultra-high performance fibre reinforced concrete (UHPFRC)," *Materials and Structures*. Springer, **47**(3), pp. 475–491.

Shen, X. and Brühwiler, E. (2020) "Biaxial flexural fatigue behavior of strain-hardening UHPFRC thin slab elements," *International journal of fatigue*. Elsevier, **138**, p. 105727.

Shirzadeh, R. *et al.* (2013) "Experimental and computational damping estimation of an offshore wind turbine on a monopile foundation," *Journal of Wind Engineering and Industrial Aerodynamics*, **120**(SEPTEMBER), pp. 96–106.

Velarde, J. *et al.* (2020) "Fatigue reliability of large monopiles for offshore wind turbines," *International journal of fatigue*. Elsevier, **134**(July 2019), p. 105487.

Wang, S., Larsen, T. J. and Bredmose, H. (2021) "Ultimate load analysis of a 10 MW offshore monopile wind turbine incorporating fully nonlinear irregular wave kinematics," *Marine Structures*. Elsevier Ltd, **76**(April 2020), p. 102922.

Wu, X., Yang, J. and Mpalla, I. B. (2013) "Preliminary design and structural responses of typical hybrid wind tower made of ultra high performance cementitious composites," *Structural engineering and mechanics : An international journal*. dbpia.co.kr, **48**(6), pp. 791–807.

Yang, Y. *et al.* (2020) "Mitigation of coupled wind-wave-earthquake responses of a 10 MW fixed-bottom offshore wind turbine," *Renewable Energy*. Elsevier, **157**, pp. 1171–1184.